OFF-DESIGN CHARACTERISATION OF AN ENERGY STORAGE BASED ON PUMPED THERMAL ENERGY STORAGE AND LOW-CONCENTRATION SOLAR THERMAL COLLECTORS

Guido Francesco Frate, Andrea Baccioli*, Leonardo Bernardini and Lorenzo Ferrari

University of Pisa, Department of Energy, System, Territory and Construction Engineering (DESTEC), Pisa, Italy

*Corresponding Author: andrea.baccioli@unipi.it

ABSTRACT

Long duration storages (i.e. 6+*h*) could foster the power sector transitions towards renewable energy sources. Among the many technologies proposed for such a task, pumped thermal electricity storage (PTES) recently gained much attention from researchers. A PTES plant based on low-concentration solar collectors, a vapour compression heat pump, and an organic Rankine cycle (ORC) is studied. In the proposed configuration, the solar collectors produce the thermal energy required by the heat pump during the charging phase. The heat pump operates with a reduced temperature lift and upgrades the solar thermal energy to store it at a higher temperature in sensible heat storage. The electric roundtrip efficiency is very high when the thermal energy is discharged through the ORC, thanks to solar thermal energy contribution. In the paper, the system performance in and off-design are analysed. An off-design model is used to map both heat pump and ORC for a set of representative operating conditions. Such performance maps were then used to characterise the system performance when coupled with a solar thermal energy production profile. In this way, the whole system operation was simulated for some representative days of the year. Results show that the average round trip efficiency is between 0.85 and 0.87, and the system can operate in various radiation conditions.

1 INTRODUCTION

In the European Union, the power sector produces more than 75% of greenhouse gas emissions. Therefore, increasing the power produced by renewable energy sources (RESs) is crucial to achieving carbon neutrality by 2050. Electric energy storage enables RES growth and power sector decarbonisation, as it provides the resilience often lacked by the non-dispatchable RES (Palizban and Kauhaniemi, 2016), primarily based on solar and wind energy.

Researchers still debate the most appropriate technologies for each application, and many alternatives are under scrutiny(Argyrou et al., 2018). A technology that recently gained interest for long-duration applications (6+ *h* of storage) is Pumped Thermal Energy Storage (PTES) (Dumont et al., 2020).

PTES stores electric energy as thermal exergy and, even though it usually achieve roundtrip efficiencies lower than electrochemical storage, features promising cost per kWh and employs environmentally benign materials. Furthermore, since PTES stores thermal exergy (i.e. heat, in most cases), it can synergically interact with systems where both heat and power are produced or required (Steinmann et al., 2019). The PTES can be powered by electrical inputs and additional thermal exergy sources in such contexts, leading to improved electrical roundtrip efficiency (Frate et al., 2017). In the literature, this application is known as Thermal Integration (TI) (Frate et al., 2020a) and was proposed for thermal exergy sources like district heating networks (DHNs), solar collectors (Bellos et al., 2021), geothermal wells and Waste Heat Recovery (WHR) (Dumont et al., 2020).

The TI thermodynamic effectiveness is mainly based on the thermal exergy source temperature level. However, with different sources, there are different technical and economic issues: in DHNs and WHR, the thermal exergy may be readily available, while, for solar and geothermal sources, it is necessary to build a costly infrastructure to exploit the resource. In exchange, with solar and geothermal sources, the TI-PTES plant is not bounded to the specific location where the thermal exergy is already produced (Frate et al., 2020a). Quantifying the impact of these issues is not an easy task, which has never been

performed comprehensively to the best of the authors' knowledge. The coupling between TI-PTES systems and renewable electric energy sources (Sànchez-Canales et al., 2020) or electric demand profiles (Eppinger et al., 2021) has been previously investigated. However, these studies do not consider heat source availability an operational constraint for the investigated TI-PTES system. On the contrary, this may significantly limit the annual operating time and should be considered.
The present paper considers the interaction between the TI-PTES and a solar thermal source and provides a detailed assessment of a solar-based TI-PTES plant thermodynamic performance as an original contribution to this broader research quest.
Based on previous studies (Frate et al., 2020b), a TI-PTES system based on a vapour-compression High-Temperature Heat Pump (HTHP), a sensible Thermal Exergy Storage (TES) and an Organic Rankine Cycle (ORC) is studied. In the system, the solar thermal exergy powers up the HTHP evaporator during the charging phase. In this way, the HTHP operates with a reduced temperature lift, i.e. with an increased COP, and the electrical roundtrip efficiency is improved.
Both the design and off-design system operation are modelled to consider the solar resource fluctuating behaviour. HTHP and ORC off-design models were developed to this end, and their performance was mapped for several operating conditions. Such performance mappings were used in the system simulation, which also considered the solar field thermal inertia and simplified control logic.
Several software tools were used for the study: design and off-design analyses of both HTHP and ORC were conducted in ASPEN HYSYS to obtain the operating maps, whereas system simulations were performed in MATLAB.
For the simulation, a case study from south Spain, a region with abundant solar resources, is selected, and the plant operation was simulated for three months (January, April, and July) to consider the solar resource variation along the year.

2 METHODOLOGY

2.1 Solar TI-PTES plant layout

The system layout is reported in Figure 1. The HTHP is powered by the thermal energy from the Concentrated Parabolic Collectors (CPCs) and the electric energy from the grid power in the charging phase and converts both into thermal exergy stored in the Thermal Exergy Storage (TES). The TES exergy is converted into power by the Organic Rankine Cycle (ORC) in the discharging phase. A detailed description of the TI-PTES operating principle is in (Frate et al., 2020a).
Although it is possible to conceive different layouts that directly store the solar thermal energy in the TES or directly convert it into power with the ORC, they are not considered in the study.

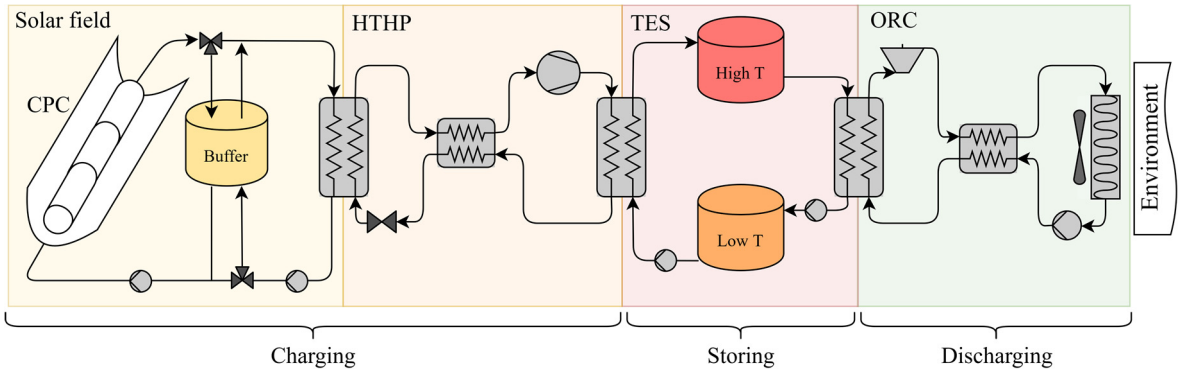

Figure 1: Solar TI-PTES plant layout.

2.2 Solar TI-PTES component sizing

Previous studies (Frate et al., 2020c) demonstrated that TI-PTES systems achieve similar performance with different HTHP and ORC operating fluid combinations. Here, Pentane is selected for the HTHP and R245fa for the ORC. For the TES, which operates as sensible heat storage, the Therminol 55 thermal oil is used. Finally, for the CPCs, pressurised water is selected as a heat carrier fluid.

During TI-PTES design, the HTHP, ORC, and TES operating temperatures can be manipulated to maximise thermodynamic, technical, or economic KPIs (Frate et al., 2020b, 2020c). The cited analyses demonstrated how designing the system for the maximum electrical roundtrip efficiency may lead to unrealistic designs from technical or economic standpoints. In solar TI-PTEs systems, maximising the electrical roundtrip efficiency would lead to an unrealistically sizeable solar field since the electrical roundtrip efficiency gives no value to the CPC thermal output. In this regard, further details are discussed in (Frate et al., 2017).
Although technical and economic KPIs are not explicitly considered in the TI-PTES design, unfeasible configurations are ruled out by giving importance to *both* electrical and thermal inputs/outputs. Therefore, the proposed TI-PTES design maximises the second-law (exergy) efficiency ψ, which properly accounts for the fact that both thermal and electric inputs/outputs are used/produced. Indeed, a similar result can be achieved by designing the system to minimise a specific economic objective function (i.e. the cost per kWh or per kW). However, an economic analysis may entail a significant uncertainty since the component costs and electric energy prices are not always known or depend on the specific case study. In this preliminary study, for generality, TI-PTES design was based purely on technical and thermodynamic considerations.
For TI-PTES systems, the exergy efficiency ψ is defined as in equation (1):

$$\psi = \frac{W_{orc}}{Ex_{cpc}+W_{hp}} \tag{1}$$

W_{orc} and W_{hp} are the net HTHP and ORC electric output and input, and Ex_{cpc} is the thermal exergy produced by the CPCs. It is worth noting that ψ does not consider the exergy losses inside the CPC, which characterise solar radiation conversion into thermal exergy, as they are assumed as unavoidable when CPCs are used. In equation (1), W_{orc} already considers ORC pump and condenser fan auxiliary consumption, while both W_{orc} and W_{hp} are calculated considering electrical and mechanical losses in the generator, motor, HTHP compressor and ORC expander. Other minor auxiliary consumptions, e.g. TES and CPC circulating pumps, were neglected.
The electric roundtrip efficiency ε is defined as in equation (2):

$$\varepsilon = \frac{W_{orc}}{W_{hp}} = \frac{\int_0^{\tau_{hp}} \dot{W}_{hp}\, dt}{\int_0^{\tau_{orc}} \dot{W}_{orc}\, dt} \tag{2}$$

$\dot{W}_{hp}$ and $\dot{W}_{orc}$ are HTHP and ORC power input and output, respectively, and τ_{hp} and τ_{orc} are the charging and discharging phase durations.
The CPC area A_{cpc} is calculated from the solar collector energy balance in steady-state conditions, with the hypothesis that the HTHP evaporator absorbs all the CPC thermal energy and no buffer is used (equation (3)):

$$\dot{Q}_{cpc} = \left(I_b + \frac{I_d}{C}\right) \cdot A_{cpc} \cdot \eta_{cpc} = \dot{Q}_{eva,hp} \tag{3}$$

where I_b and I_d are the beam and diffuse solar radiation components respectively, evaluated for a tilted surface, and η_{cpc} is the collector efficiency, calculated as in equation (4):

$$\eta_{cpc} = \eta_{opt} - a_1 \cdot \frac{(T_{cpc,ave}-T_{ext})}{I_b+\frac{I_d}{C}} - a_2 \cdot \frac{(T_{cpc,ave}-T_{ext})^2}{I_b+\frac{I_d}{C}} \tag{4}$$

η_{opt} is the CPC optical efficiency, $T_{cpc,ave}$ is the average CPC temperature between inlet and outlet, T_{ext} is the environment temperature, a_1 and a_2 are characteristic CPC constants, and C is the concentration degree.
The quantities in equation (1) – (4) and the HTHP and ORC characteristic parameters such as machine isentropic efficiencies and maximum/minimum operating temperatures are kept constant during the

system sizing. Such parameters are reported in Table 1. In the analysis, the adopted heat exchanger technology is the corrugated plate one.
The sizing optimisation problem variables are the HTHP and ORC evaporating and condensing temperatures, the subcooling and superheating degree at the HTHP evaporator and condenser outlets, the superheating degree at the ORC evaporator outlet, the maximum TES temperature, and the inlet and outlet CPC operating fluid temperatures.
For a complete system optimisation, several effects should be considered. In particular, the HTHP condensation temperature should not be too high. It is true that the higher the HTHP condensing temperature, the higher the TES temperature and the ORC efficiency (which measures the discharging effectiveness). However, operating with high condensing temperatures usually implies having higher pressure and volume ratios on the compressor, leading to lower isentropic efficiencies, higher TES costs and lower HTHP COP (which measures the charging effectiveness). These considerations seem to point towards low HTHP condensing temperatures (for example, to maximise COP and ε). However, the difference between HTHP evaporating and condensing temperatures should not be too low since operating with a high COP implies a larger solar field area. This is because, with high COP, a larger heat flow rate is required for each charged electric kWh. Since the solar field is a costly component, maximising the efficiency could lead to unrealistically costly configurations. Therefore, a balance should be searched between the different effects described above.
The optimisation problem is subject to some constraints, which guarantee the observance of each component energy balance, avoid any temperature cross in the heat exchangers, and maintain the HTHP and ORC operating temperatures and pressures within a technically feasible range. Furthermore, the difference between the CPC inlet and outlet temperature cannot be lower than 10 K to avoid operating with excessively high mass flow rates. The HTHP and ORC were modelled in Aspen Hysis®, and the system was optimised using the software optimisation utilities. Further details on the optimisation problem are not provided for the sake of brevity.

Table 1: HTHP, ORC, CPC and TES characteristic parameters

HTHP			ORC				CPC				TES
$\eta_{is,cmp}$ [-]	T_{max} [°C]	$\Delta T_{pp,hp}$ [K]	$\eta_{is,exp}$ [-]	$\eta_{is,pmp}$ [-]	$\eta_{is,fan}$ [-]	$\Delta T_{pp,orc}$ [K]	η_{opt} [-]	a_1 [$Wm^{-2}K^{-1}$]	a_2 [$Wm^{-2}K^{-2}$]	C [-]	ΔT_{tes} [K]
0.8	180	2	0.85	0.7	0.6	2	0.63	0.885	0.001	1.25	30

In the study, a solar TI-PTES system with nominal $\dot{W}_{hp}$ equal to 50 kW was considered. The nominal τ_{hp} was set to 8 h, while the discharge one τ_{orc} to 4 h. Based on these assumptions and the outlined design procedure, the resulting solar TI-PTES is reported in Table 2.

Table 2: solar TI-PTES system specifications

$\dot{W}_{hp}$ [kW]	τ_{hp} [h]	COP_{hp} [-]	$\dot{W}_{orc}$ [kW]	τ_{orc} [h]	η_{orc} [-]	V_{tes} [m^3]	ε [-]	ψ [-]	A_{cpc} [m^2]	$T_{cpc,in}$ [°C]	$T_{cpc,out}$ [°C]	$T_{tes,max}$ [°C]
50	8	5.9	83	4	0.14	310	0.83	0.39	630	104	119	151

2.3 HTHP and ORC off-design modelling

The use of solar energy forces the TI-PTES system to operate continuously in off-design. Furthermore, a storage system must be able to operate in part-load. Therefore, it is essential to consider the HTHP and ORC off-design performance to simulate the impact of solar energy utilisation on the TI-PTES operation realistically.
For the heat exchangers, varying heat transfer coefficients and pressure drops are considered using equation (5) and (6):

$$\alpha_{off} = \alpha_{des} \cdot \left(\frac{\dot{m}_{des}}{\dot{m}_{off}}\right)^{0.8} \quad (5)$$

$$\Delta p_{off} = \Delta p_{des} \cdot \left(\frac{\dot{m}_{off}}{\dot{m}_{des}}\right)^2 \cdot \frac{\rho_{des}}{\rho_{off}} \tag{6}$$

where *off* and *des* subscripts identify off-design and design conditions, respectively. α is the convective heat transfer coefficient, Δp is the pressure drop, $\dot{m}$ is the mass flow rate and ρ fluid density at the heat exchanger inlet. In design conditions, α and Δp are calculated using Aspen EDR® heat exchanger design utility.

For the HTHP compressor, the operating map in Figure 2 was used to account for off-design performance and calculate the pressure ratio β and isentropic efficiency $\eta_{is,cmp}$ for any given combination of RPM and volumetric flow rate $\dot{V}_{cmp}$ at compressor suction. Even though the outlined methodology can be followed for any compressing technology, the map in Figure 2 refers to a screw compressor. Such compressor technology is suited for HTHP applications and can be applied for the size range investigated in the paper.

The simplified modelling approach presented in (Frate et al., 2021a) was used for the ORC expander. A turboexpander is used in the system, which results in higher efficiencies in design conditions for the investigated ORC size range. The relationship for choked turbines (Cooke, 1985) was used, as the ORC always operates with an expansion ratio beyond the critical one in this case. Therefore, the turbine inlet pressure $p_{exp,in}$ in off-design can be calculated from the fluid mass flow rate and the inlet density as in equation (7):

$$p_{exp,in,off} = p_{exp,in,des} \cdot \frac{\dot{m}_{off}}{\dot{m}_{des}} \cdot \frac{\rho_{des}}{\rho_{off}} \tag{7}$$

Finally, the approach in (Manente et al., 2013) was adopted to calculate the off-design isentropic efficiency, which varies according to the expander operating conditions. Since the characteristic curve was analytically calculated, no expander operating maps were used in the analysis. Based on the provided modelling, the HTHP off-design performance was mapped for several combinations of CPC output temperature and heat flow rate provided to the TES (i.e. the HTHP thermal load). The results of such mapping are reported in Figure 3. Similarly, the ORC off-design performance was mapped for several combinations of environmental temperature T_{ext} and heat flow rate provided by the TES (i.e. the thermal load provided to the ORC). Constant superheating and oil temperature at the heat pump condenser were imposed for the HTHP while sliding pressure was chosen as a control strategy for ORC by keeping the superheating grade constant. The results of such mapping are reported in Figure 4. It is worth noting that it is assumed that the TES temperatures do not vary despite the off-design operation. Therefore, the HTHP and ORC performance are not mapped for different $T_{tes,max}$ and $T_{tes,min}$ values.

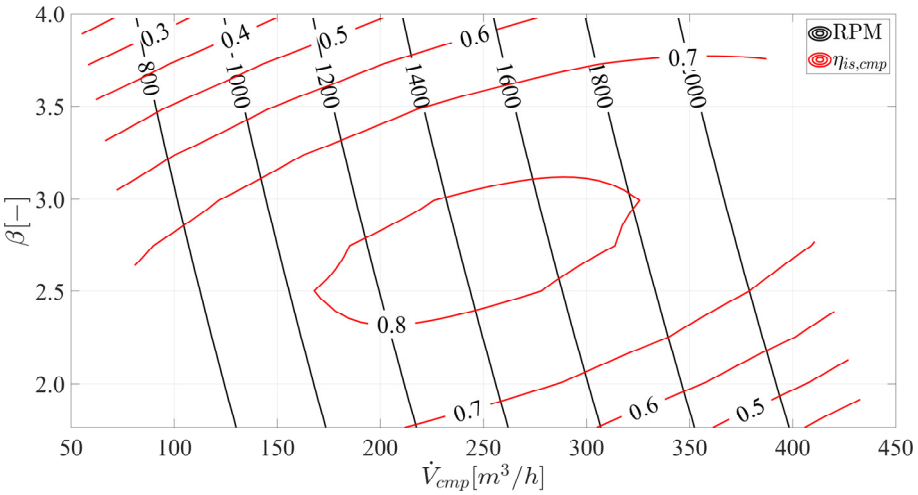

Figure 2: HTHP compressor operating map. On the y-axis, the compressor pressure ratio (β). On the x-axis, the volumetric flow rate at compressor suction in m^3/s.

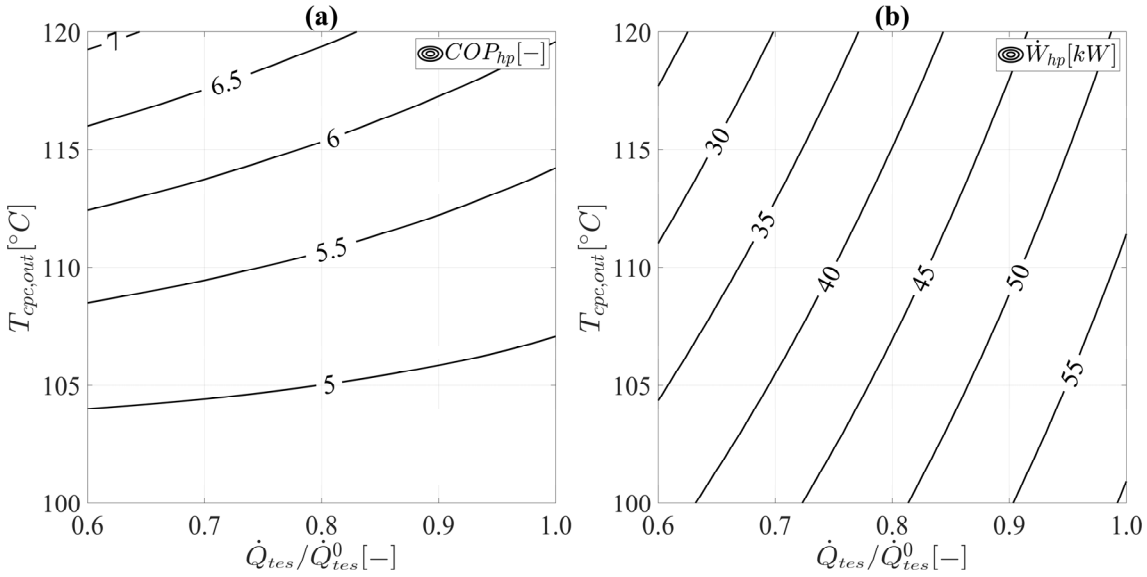

Figure 3: HTHP operating maps for different values of $T_{cpc,out}$ and relative thermal load provided to the TES $\dot{Q}_{tes}/\dot{Q}^0_{tes}$. (a): COP_{hp}. (b): $\dot{W}_{hp}$

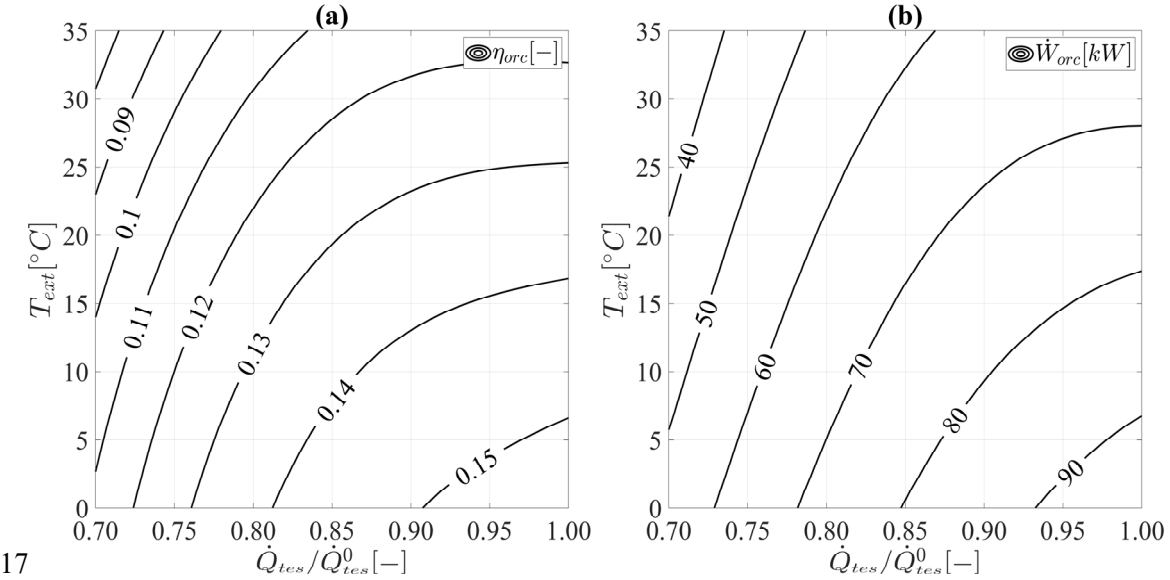

17

Figure 4: ORC operating maps for different T_{ext} values and relative thermal load provided by the TES $\dot{Q}_{tes}/\dot{Q}^0_{tes}$. (a): η_{orc}. (b): $\dot{W}_{orc}$.

2.4 Charging phase modelling and simulation

During the charging phase, only the solar collector field and the HTHP are operated. The solar collector dynamic behaviour was considered, to realistically account for the impact of the system thermal capacities and control strategy. The subsystem made up of the solar collectors, buffer tank, and heat pump evaporator (Figure 5) has been modelled and simulated in MATLAB by defining the mass and energy balance of both the solar field and buffer storage tank. The buffer tank is assumed to be perfectly mixed, which makes the buffer internal temperature distribution easily calculable. This hypothesis is conservative, as a thermocline temperature internal distribution would have reduced the system exergy destruction.

In the charging phase, the heat pump behaviour is based on the performance mappings in Figure 3. A time step of 10 minutes was adopted to discretise the time derivatives accurately and consider a steady-state heat pump operation. Pressurised water was used as the Heat Transfer Fluid (HTF) in the loop.
The system operation is controlled by using two variable speed pumps and a set of controllable mixing valves. Such equipment allows varying the mass flow rates circulating in the branches represented in Figure 5 while also maintaining an adequate temperature level at the heat pump evaporator inlet ($T_{hp,in}$). The system is controlled as outlined below: Referring to Figure 5 nomenclature:

- while the outlet collector temperature $T_{cpc,out} \leq T_{cpc-on}$, with $T_{cpc\text{-}on}$ = 85 °C, then the system is shut down, and the mass flow rates in all the branches are zero;
- while $T_{cpc,out} > T_{cpc-on}$ (i.e. the CPC is operating) and $T_{cpc,out} \leq T_{bf}$ (i.e. the CPC cannot charge the buffer) the HTF fluid is circulated within the CPC, bypassing the other components. Therefore, all the mass flow rates are zero except for $\dot{m}_{cpc}$ and $\dot{m}_{byp}$;
- when the CPC outlet becomes warmer than the buffer ($T_{cpc,out} > T_{bf}$), the last is charged until its temperature reaches the HP-activation threshold, $T_{bf} > T_{bf,hp-on}$, with $T_{hp\text{-}on}$ = 110 °C. All the mass flow rates except those in the branches connecting the CPC and the buffer are set to zero during this phase;
- when $T_{bf} > T_{bf,hp-on}$ the buffer charging stops, and the CPC directly powers the HTHP evaporator. In this case, until $T_{cpc,out} \leq \bar{T}_{hp,in}$, (i.e. until the CPC outlet temperature has not reached the setpoint $\bar{T}_{hp,in}$ = 120 °C) all the mass flow rates except those in the branches connecting the CPC and the HTHP are set to zero (the buffer is not charged nor discharged);
- while $T_{cpc,out} = \bar{T}_{hp,in}$ the system operates in its design conditions. When the solar radiation is too intense, the excess heat flow rate is stored in the buffer (Figure 6 *f* shows the buffer initial and subsequent charging phases up to around 120 °C). In these operating conditions, the mass flow rates in the branches that connect the CPC with the buffer and the CPC with the HTHP are non-zero;
- when the $T_{cpc,out} \leq T_{bf} - \Delta$, with Δ = 2 K, the buffer starts to power up the HTHP, while the CPC mass flow rate is recirculated through the bypass. In this configuration, the mass flow rates in the branches between the HTHP and the CPC are set to zero, while the HTF circulates in the HTHP-buffer and CPC-bypass loops. If CPC outlet temperature increases again ($T_{cpc,out} > T_{bf} + \Delta$), the direct connection between the CPC and the HTHP is re-established, and the buffer stops powering the HTHP evaporator;
- when both and $T_{bf} < T_{bf,hp-off}$ and $T_{cpc,out} < T_{bf}$, with $T_{bf,hp\text{-}off}$ = 105 °C, the charging phase stops, and the HTF circulates only in the CPC and the bypass;
- Finally, when $T_{cpc,out} < T_{cpc-off}$ the system shuts down, with $T_{cpc\text{-}off}$ = 80 °C.

As for the TES, the temperature is kept constant at 150 °C by adjusting the heat pump operation. The heat pump electric load was assumed as equal to the minimum load (60%) in the first and last hours of the day, while a sinusoidal profile was provided for the central hours to approximately match both the collector load profile and the projected electric surplus daily trend which would be driven by PV production.

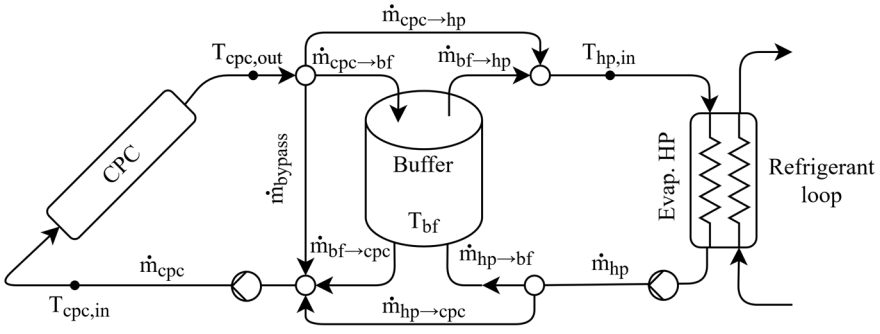

Figure 5: Solar collector field conceptual scheme during the charging phase.

2.5 Case study

The system was simulated for fifteen continuous days of January, April and July. These three months can be considered representative of winter, summer, and mid-season conditions. The beam and diffuse radiation profiles are taken from the PVGIS dataset (European Commission Joint Research Center, 2021) and refer to Guadix (Granada, Spain), where the Andasol power plant is built.

3 RESULTS

As it resulted, the TI-PTES system was able to charge for all the considered July and April days (Fig. 6 a). In January, the system was turned off in two days only due to the low radiation (Fig. 6 d). Relying purely on solar radiation may not be a problem if the system is conceived as storage for systems with a high PV installed capacity: when the solar radiation is too low, there is no need for storing energy. Focusing daily operation (Fig. 6 b, c, e, f), a significant solar field outlet temperature fluctuation over time can be noticed. This behaviour is due to the bypass valve control: buffer bypass is enabled when the solar field outlet temperature is above 90 °C, and the buffer temperature is above 120 °C. When the radiation is low, e.g. in winter, collector temperature can decrease below the lower trigger threshold, causing the bypass valve to close. In this condition, the buffer starts to power the heat pump. Consequently, the solar field is fed by a higher temperature flow from the bypass, causing the outlet temperature to increase, leading to opening the bypass valve again. This cycle may repeat until solar radiation is not intense enough to heat the fluid above the buffer temperature. From this situation onwards, the heat pump is powered only by the buffer until it is discharged.

As from Fig. 6, the heat pump operating temperature profiles are almost constant in July, and the solar field outlet temperature is often equal to its maximum value (120 ° C). Therefore, the heat pump operates most of the time and at a high average COP (Fig. 7 b). The operation time is significantly shorter in winter than in summer (Fig. 7 d), but the system could charge when solar radiation reached high values. Due to the average lower temperatures reached in winter, the average COP achieved by the heat pump is slightly smaller than in the other months (Fig. 7 b)

As for the discharging phase, the ORC achieved the best efficiency in winter due to the low ambient temperatures that reduce the condensing pressure. As a result, the average round trip efficiency results maximum in winter rather than in summer (Fig. 7 a). As for the operating time and stored energy, the charge phase is longer in summer than in winter due to the more prolonged insolation hours. More extended daylight periods affects both the operating hours and the charged energy, which almost doubled from winter to summer (Fig. 7 d and e). However, even in winter, the system operated for five hours per day on average (Fig. 7 d). Such a result confirms that the proposed system is suitable for electric energy storage for PV systems in all seasons. Finally, since the system is sized for summer production, even the discharging phase becomes longer in July due to the amount of thermal energy charged in the tank.

4 CONCLUSIONS

In this study, the behaviour of a solar TI-PTES under actual operating conditions has been tested. The system is composed of a solar-heated high-temperature heat pump, a storage tank, and an ORC. The heat pump and ORC design and off-design conditions were obtained through an Aspen Hysys model by considering all the main system components. Results from Hysys simulations were used in a Matlab model to simulate the TI-PTES under fluctuating radiation conditions. The system proved to be efficient (round trip between 0.85 and 0.87) and flexible in all the tested conditions, making the solar PTES a viable option as storage for systems with a high installed PV capacity.

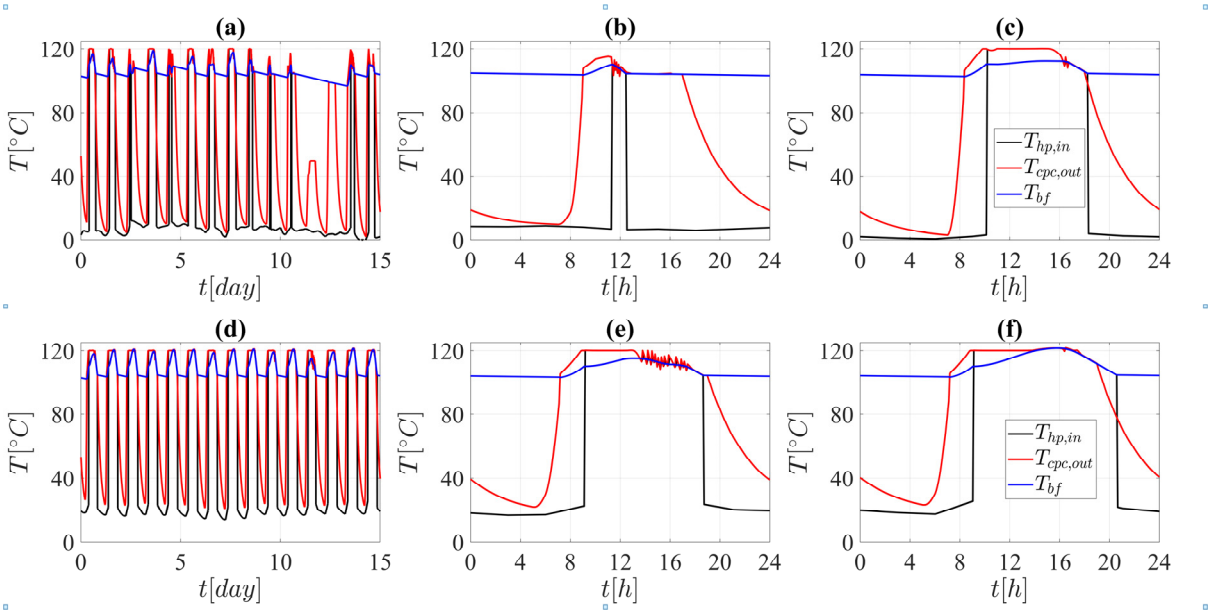

Figure 6: Temperature trends for the solar field outlet, buffer and HTHP inlet. (a – c): January. (d – f): July. (a and d): the first 15 days of the month. (b and e): a day with low production. (c and f): a day with high production.

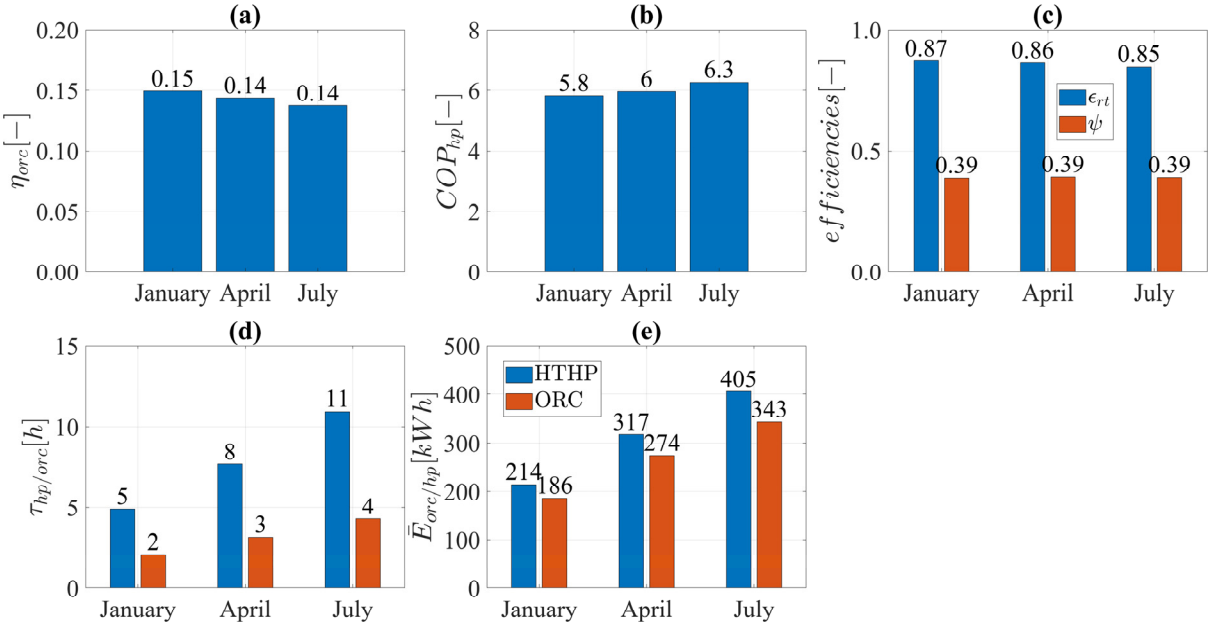

Figure 7: Daily average results. (a): ORC efficiency. (b): HTHP COP. (c): roundtrip and exergy efficiency. (d): daily operating hours. (e): daily charged and discharged electric energy.

NOMENCLATURE

Symbol

ψ	exergy efficiency	(-)
ε	electrical roundtrip efficiency	(-)
η	efficiency	(-)

Subscript

bf	CPC buffer
cpc	compound parabolic collector
hp	heat pump

on/off	on and off thresholds for the related component
opt	optical
orc	organic Rankine cycle
tes	thermal exergy storage

REFERENCES

Argyrou, M. C., Christodoulides, P., and Kalogirou, S. A. (2018). Energy storage for electricity generation and related processes: Technologies appraisal and grid scale applications. *Renew. Sustain. Energy Rev.* 94, 804–821. doi:10.1016/j.rser.2018.06.044.

Bellos, E., Tzivanidis, C., and Said, Z. (2021). Investigation and optimisation of a solar-assisted pumped thermal energy storage system with flat plate collectors. *Energy Convers. Manag.* 237, 114137. doi:10.1016/j.enconman.2021.114137.

Cooke, D. H. (1985). On Prediction of Off-Design Multistage Turbine Pressures by Stodola's Ellipse. *J. Eng. Gas Turbines Power* 107, 596–606. doi:10.1115/1.3239778.

Dumont, O., Frate, G. F., Pillai, A., Lecompte, S., De paepe, M., and Lemort, V. (2020). Carnot battery technology: A state-of-the-art review. *J. Energy Storage* 32, 101756. doi:10.1016/j.est.2020.101756.

Eppinger, B., Muradi, M., Scharrer, D., Zigan, L., Bazan, P., German, R., et al. (2021). Simulation of the Part Load Behavior of Combined Heat Pump-Organic Rankine Cycle Systems. *Energies* 14, 3870. doi:10.3390/en14133870.

European Commission Joint Research Center (2021). Photovoltaic Geographical Information System (PVGIS). Available at: http://re.jrc.ec.europa.eu/pvg_tools/en/tools.html#TMY [Accessed February 4, 2021].

Frate, G. F., Antonelli, M., and Desideri, U. (2017). A novel Pumped Thermal Electricity Storage (PTES) system with thermal integration. *Appl. Therm. Eng.* 121, 1051–1058. doi:10.1016/j.applthermaleng.2017.04.127.

Frate, G. F., Ferrari, L., and Desideri, U. (2020a). Rankine Carnot Batteries with the Integration of Thermal Energy Sources : A Review. *Energies* 13, 4766. doi:10.3390/en13184766.

Frate, G. F., Ferrari, L., and Desideri, U. (2020b). Multi-Criteria Economic Analysis of a Pumped Thermal Electricity Storage (PTES) With Thermal Integration. *Front. Energy Res.* 8. doi:10.3389/fenrg.2020.00053.

Frate, G. F., Ferrari, L., and Desideri, U. (2020c). Multi-criteria investigation of a pumped thermal electricity storage (PTES) system with thermal integration and sensible heat storage. *Energy Convers. Manag.* 208, 112530. doi:10.1016/j.enconman.2020.112530.

Manente, G., Toffolo, A., Lazzaretto, A., and Paci, M. (2013). An Organic Rankine Cycle off-design model for the search of the optimal control strategy. *Energy* 58, 97–106. doi:10.1016/j.energy.2012.12.035.

Palizban, O., and Kauhaniemi, K. (2016). Energy storage systems in modern grids—Matrix of technologies and applications. *J. Energy Storage* 6, 248–259. doi:10.1016/j.est.2016.02.001.

Sànchez-Canales, V., Payà, J., Corberàan, J. M., and Hassan, A. H. (2020). Dynamic Modelling and Techno-Economic Assessment of a Compressed Heat Energy Storage System : Application in a 26-MW Wind Farm in Spain. *Energies*. doi:https://doi.org/10.3390/en13184739.

Steinmann, W. D., Bauer, D., Jockenhöfer, H., and Johnson, M. (2019). Pumped thermal energy storage (PTES) as smart sector-coupling technology for heat and electricity. *Energy* 183, 185–190. doi:10.1016/j.energy.2019.06.058.